Engineering Fracture Mechanics 206 (2019) 250–266

Contents lists available at ScienceDirect

Engineering Fracture Mechanics

journal homepage: www.elsevier.com/locate/engfracmech

Use of the stress gradient factor to estimate fatigue stress concentration factors K_f

Antonio Carlos de Oliveira Miranda[a,*], Marcelo Avelar Antunes[a], Marco Vinicio Guamán Alarcón[b], Marco Antonio Meggiolaro[c], Jaime Tupiassú Pinho de Castro[c]

[a] Department of Civil and Environmental Engineering, University of Brasília, SG-12 Building, Darcy Ribeiro Campus, DF 70.910-900, Brazil
[b] Department of Mechanical Engineering, Escuela Politécnica Nacional, 170525 Quito, Ecuador
[c] Mechanical Engineering Department, Pontifical Catholic University of Rio de Janeiro, Rua Marquês de São Vicente 225 – Gávea, Rio de Janeiro, RJ 22451-900, Brazil

ARTICLE INFO

Keywords:
Fracture mechanics
Stress concentration factor
Stress gradient factor
Notch factor

ABSTRACT

Stress concentration effects in unavoidable notches reduce fatigue strengths and lives of most structural components, so they must be properly quantified when designing and analyzing them. The Stress Gradient Method (SGM), based on classic Fracture Mechanics concepts and on short crack ideas, can be used to calculate Stress Gradient Factors (SGF) and to properly estimate fatigue stress concentration factors K_f. The procedures proposed here to calculate them are general and only require the normal stress distribution ahead of the notch tip and material properties. The SGF concept is defined to differentiate it from the geometric stress concentration factor K_t, also present in stress intensity factor equations for cracks. Using short crack, SGM concepts, and SGF, a general equation is proposed to compute K_f, which is discretized to be used with any numerical methods (a short C++ algorithm is presented to solve it). Experimental K_f data are used to validate the proposed method, showing good agreement with its predictions, especially for sharp notches.

1. Introduction

It is well known that fatigue damage depends on two driving forces. Fatigue crack initiation is driven by the history of stress or strain ranges $\Delta\sigma$ or $\Delta\varepsilon$ and by their stress peaks σ_{max} acting at the critical point of structural components, usually a notch tip, so both are much affected by the stress concentration factor (SCF) K_t induced by the notch. Fatigue crack growth (FCG), on the other hand, is driven by the history of the stress intensity factor (SIF) ranges and peaks ΔK and K_{max} of the crack that departs from the notch tip, which are affected by the stress concentration field induced by the notch. Likewise, the mechanical driving forces for environmentally assisted cracking (EAC) problems are the peak of the critical stress to start a crack at a notch tip, and the peak of that crack SIF to propagate it. Therefore, the damage induced by such mechanisms can (and usually should) be modeled as a local problem, where stress concentration effects induced by sharp geometric variations (caused by holes, slots, grooves, keyways, shoulders, corners, threads, weld fillets, reinforcements, etc., generically called notches) play a very significant role.

Due to their major practical importance, many methodologies have been proposed to include short crack effects in fatigue life

* Corresponding author.
E-mail addresses: acmiranda@unb.br (A.C. de Oliveira Miranda), marco.guaman@epn.edu.ec (M.V. Guamán Alarcón), meggi@puc-rio.br (M.A. Meggiolaro), jtcastro@puc-rio.br (J.T. Pinho de Castro).

https://doi.org/10.1016/j.engfracmech.2018.11.049
Received 30 August 2018; Received in revised form 21 November 2018; Accepted 26 November 2018
Available online 05 December 2018
0013-7944/

Nomenclature

Abbreviations and Nomenclatures

CNBT	Circumferential V-shaped notch in a round bar under remote tension
CNP	Center-notched plate
CNPT	Center-notched plate under remote tension
DNPT	Double edge-notched plate under remote tension
DSGM	Direct stress gradient method
ENP	Edge-notched plate
ESCF	Elastic stress concentration factor
FCG	Fatigue crack growth
FE	Finite elements
LEFM	Linear Elastic Fracture Mechanics
LM	Liu and Mahadevan's methodology
MSCF	Modified stress concentration factor
SBFM	Strain-based fracture mechanics
SGF	Stress Gradient Factor
SGM	Stress Gradient Method
SIF	Stress intensity factor
TCD	Theory of critical distance
a	Crack length
a_0	Short crack characteristic size for R = 0
a_i	i_{th} discretized crack length
a_R	Short crack characteristic size at a given R
a_{max}	Crack size that limits propagation/non-propagation of short cracks
d_i	i_{th} discretized distance
$f(a/w)$	Geometry factor
K_f	Fatigue stress concentration factor
$K_{gr}(a/w)$	Stress gradient factor
$K_{gr,i}$	i_{th} discretized stress gradient factor
K_I	Stress intensity factor, mode I
$K_{I(ref)}$	Reference stress intensity factor
K_{max}	Maximum stress intensity factor
K_t	Stress concentration factor
P_i	i_{th} discretized force
q	Notch sensitivity factor
ρ	Notch radius
R	Load radio
w	Width
γ	Bazant's adjustable parameter
ΔK	Stress intensity factor range
ΔK_0	Fatigue crack growth threshold for R = 0
ΔK_{th}	Fatigue crack threshold
ΔS_{L0}	Fatigue crack initiation limit for R = 0
$\Delta S_{L,R}$	Fatigue crack initiation limit at a given R
$\Delta\sigma_n$	Nominal stress range
σ	Stress
σ_{max}	Maximum nominal stress

prediction models, such as the theory of critical distance (TCD) [1], the stress gradient formulation for fatigue analysis of notched components [2], and the cohesive zone model (CZM) [3]. The methodology proposed in this paper, which with minor adjustments can be extended to EAC problems, uses classic fatigue and fracture mechanics concepts to model the behavior of mechanically short cracks, larger than the grain size but not much larger than the short crack characteristic size a_0 [4–9]. In fatigue, $a_0 = (1/\pi)\cdot[\Delta K_{th}(R)/S_L(R)]^2$, where $\Delta K_{th}(R)$ and $S_L(R)$ are the FCG threshold and the fatigue limit of the material, both at a given $R = K_{min}/K_{max}$ ratio. In EAC, $a_0 = (1/\pi)\cdot[K_{EAC}/S_{EAC}]^2$, where K_{EAC} and S_{EAC} are the crack propagation and initiation thresholds of the material in the given environment.

Fatigue stress concentration factors, ideally defined by the ratio between the fatigue strengths of smooth (un-notched) and notched specimens, $K_f = S_{Lun}/S_{Lnt}$, are much used in fatigue designs and analyses of notched components to consider the actual effect of the notches on fatigue crack initiation problems, usually smaller than K_t. As described by Ciavarella and Meneghetti [10], the original K_f formulae proposed a long time ago by Neuber [11], Peterson [12], and Heywood [13], despite empirical, have many practical applications and are still recommended in fatigue design textbooks [14–18]. However, no universal K_f expression is accepted for general loading conditions, since experimental data indicate it depends on many factors, among them material properties, shape and size of inherent defects, size and geometry of the notched component, stress gradient ahead of the notch tip, loading type, and number of cycles [19]. Instead of quantifying such effects, a notch sensitivity factor is widely used to compute K_f values in practical applications, defined by

$$q = \frac{K_f - 1}{K_t - 1} \tag{1}$$

Similar expressions may be found in [19], which provides more detailed information on each formulation. However, this simple approach has some issues, since empirical K_f equations require extensive experimental calibration [10,18]. In particular, such equations are not adequate for sharp notches, and they have limitations for blunt notches [10].

Unlike the intrinsically empirical nature of classic approaches based on fatigue limit ratios, fracture mechanics-based approaches to model K_f assume that fatigue is actually a crack growth process, which depends on driving forces based on stress intensity parameters [4–9,19,20].

Navarro et al. [21] e.g. used 2D multiaxial fatigue models to deal with stress concentration effects in fatigue, combining crack initiation and propagation phases in many stress gradient scenarios without a crack length a priori. Zhuang and Molent [22] used 3D elastoplastic finite elements (FE) with a non-linear isotropic/kinematic hardening constitutive model to determine notch tip stresses, obtaining reasonable agreement with experimental results. Götz and Eulitz [23] examined empirical and semi-empirical K_f-prediction concepts and statistically evaluated steel-based powder metallurgical materials, finding better results using the TCD point method

(PM) method than a fracture mechanics-based approach [24], which yielded higher scatter and non-conservative results, with overestimated endurance limits. However, in a more recent study, Götz et al. [25] re-explored this problem and proposed an enhanced methodology using 3D models and the Support Factor Concept to overcome the weaknesses of their previous fracture mechanics-based model, ultimately obtaining better results with a fracture mechanics-based approach. Yang and Vormwald [26] recently used a linear elastic fracture mechanics-based approach in their 3D fracture analyses. They were able to obtain satisfactory results for notched components under lower loading levels, but their methodology overestimates fatigue lives for higher loading levels. Musraty et al. [27] used 3D finite element models (FEM) based on an implementation of Gurson's model [28] to assess the effectiveness of a new pipe ring notched bend specimen for determining the fracture resistance of tough pipes. Dong et al. [29] used 3D FE models and a two-phase approach to predict the total fatigue lives of notched plates.

From this brief review, it seems that while some approaches may yield satisfactory predictions for some conditions, they may fail to predict fatigue lives of notched components under others. Proper validation of fracture mechanics-based K_f models for various combinations of materials and notch geometries is still limited. While their main weakness seems to be their 3D models, Liu and Mahadevan [20] point out that it seems that fracture mechanics-based approaches have not been fully explored even for 2D methodologies.

The aim of this paper is to properly use the stress gradient factor for fatigue analyses of notched components. This idea has been successfully applied to situations where significant stress gradients were present, e.g. in welded components [30] and fretting fatigue [31–32], and it can be a sound way to compute K_f as well. Hence, this work presents a mechanically-based general methodology for fatigue analysis applicable to a wide variety of materials and notch types, which can be extended to EAC problems too. This approach considers the whole fatigue process as a crack growth problem, using only well-defined material properties and sound fracture mechanics parameters. The main ideas of this methodology are explored in Section 2, and its numerical implementation is detailed in Section 3. The proposed methodology is then validated comparing its predictions with experimental results, some of which original, in Section 4.

2. Theoretical aspects

2.1. The stress gradient factor

Fig. 1 can be used to explain the Stress Gradient Factor (SGF) concept:

Fig. 1(a) shows a Griffith plate and its SIF $K_I = \sigma\sqrt{\pi a}$, where σ is the remote nominal stress applied to the plate and $2a$ is its crack length. Fig. 1(b) shows a crack on the surface of a semi-infinite plate, whose SIF solution includes a free face factor $\eta = 1.1215$. Fig. 1(c) shows a finite strip of width w associated with a geometry factor $f(a/w)$ that accounts for its geometry and loading conditions. This $f(a/w) = 1$ when there is no crack present, that is, when $a \to 0$. Fig. 1(d) shows a plate with a notch where the crack initiates, which induces a stress concentration zone, thus a stress gradient around its tip. SIFs for cracks that depart from notch tips must account for this stress gradient, e.g. by multiplying the former solution by a SGF $K_{gr}(a/w)$, which is a function of the geometry and of the load applied to the specimen. Hence, the SGF is just a correction for a reference SIF solution that properly considers the stress gradient effects induced by the notch.

The Stress Gradient Factor (SGF) concept is based on the Elastic Stress Concentration Factor (ESCF) proposed by El Haddad and Topper [33]. First used to account for the increase in crack SIFs due to a notch or a flaw, it was then used for fatigue analyses of structural components [34,35]. El Haddad, Smith and Topper introduced Strain-based Fracture Mechanics (SBFM) concepts to extend

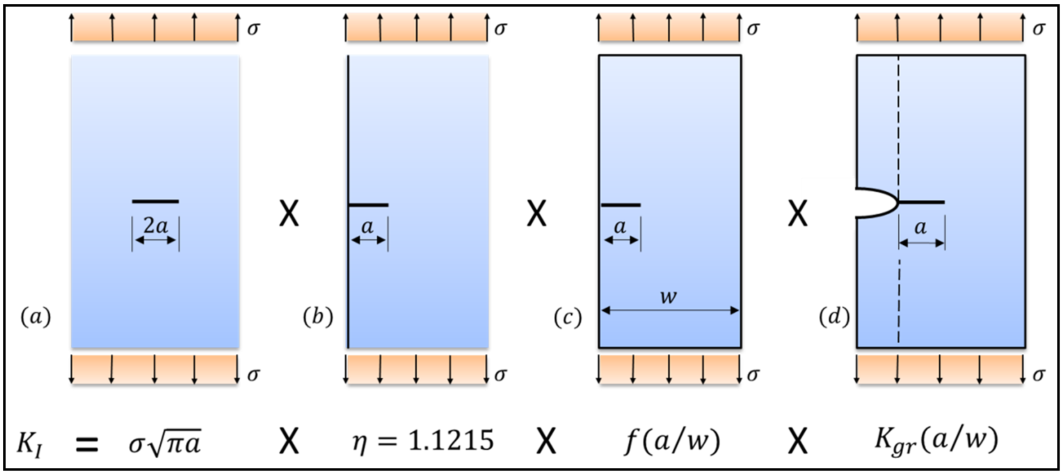

Fig. 1. The Stress Gradient Factor (SGF) concept.

it to elastoplastic conditions [36]. Ghahremani, Walbridge and Topper [30] used SBFM in fatigue analyses of weld toes under variable amplitude loads (VAL), but called the ESCF “Modified Stress Concentration Factor” (MSCF) and changed its nomenclature to K_p. Antunes et al. [31,32] proposed to unify the terms ESCF, SCF, and MSCF using the clearer notation Stress Gradient Factor K_{gr} because it modifies a reference SIF to consider the effects of stress gradients induced by notch tips, working much like a geometry factor *f(a/w)*. This is the nomenclature adopted in this article.

Generally speaking, the mode I SIF can be computed as:

$$K_I = \sigma\sqrt{\pi a}\ \prod f_i \tag{2}$$

where f_i quantify effects that affect the SIF (for instance, the free surface effect $\eta = 1.1215$ or the effects of bifurcated cracks [37,38]). Hence, for Fig. 1(d), the SIF can be calculated as:

$$K_I = \underbrace{\sigma\sqrt{\pi a}\cdot\eta}_{\Delta K_{I(ref)}}\cdot f(a/w)\cdot K_{gr}(a/w) \tag{3}$$

where $K_{I(ref)}$ is the SIF of a reference geometry, a semi-infinite strip loaded in mode I in this case, see Fig. 1(c). In other words, $K_{gr}(a/w)$ is defined by:

$$K_{gr}(a/w) = K_I/K_{I(ref)} \tag{4}$$

where K_I is computed using the approach described by Antunes et al. in [31].

Fig. 2 schematizes the effect of each f_i in Eq. (3). While the free surface factor maintains a constant value, the geometry factor *f(a/w)* starts with a unit value and grows as the crack size grows. The SGF behaves in an opposite manner, having a high initial value that tends to unit as the crack size grows. Indeed, the SGF corrects the SIF to consider notch-induced stress gradient effects that decrease as the crack tip moves away from the notch tip (or from any other features that induce stress gradients, like concentrated loads, residual stresses induced by welding or by plasticity, temperature gradients, etc.)

The differences among K_I, K_t, K_f, and K_{gr} are listed in Table 1.

2.2. K_f calculation using (mechanically) short fatigue crack and SGF concepts

El Haddad, Topper, and Smith [39,40] proposed the so-called ETS model to make FCG of short and long cracks compatible by adding a short crack characteristic size a_0 to the physical crack size of a Griffith’s plate:

$$\Delta K_I = \Delta\sigma\sqrt{\pi(a + a_0)},\qquad \text{where}\ \ a_0 = \left(\frac{1}{\pi}\right)\left(\frac{\Delta K_0}{\Delta S_{L0}}\right)^2 \tag{5}$$

This clever trick reproduces the two correct asymptotic behaviors of both the fatigue limits and the fatigue crack growth (FCG) thresholds in a Kitagawa-Takahashi (K-T) $\Delta\sigma \times a$ diagram [41]. Indeed, $\Delta\sigma(a = a_0) = \Delta S_0$ for short cracks and $\Delta K_0\ (a \gg a_0) = \Delta K_0$ for long ones (where ΔK_0 is the FCG threshold of long cracks and ΔS_{L0} is the traditional fatigue crack initiation limit, well-defined material properties measured at $R = \sigma_{min}/\sigma_{max} = 0$).

However, from conceptual as well as from operational point of views, instead of using a_0 to modify the SIFs (which should be material-independent) it is much more convenient to consider that the FCG threshold is a function of the crack size when studying the behavior of short fatigue cracks [4], using

$$\Delta K_{th}(a) = \Delta K_0\cdot[1 + (a_0/a)^{\gamma/2}]^{-1/\gamma} \tag{6}$$

where γ is a data-fitting parameter proposed by Bazant [42]. Most data for short crack FCG thresholds available in the literature can be fitted by $1.5 < \gamma < 8$ [6], as exemplified in Fig. 3.

Most K-T diagrams have been measured for pulsating loads ($R = 0$). However, FCG depends on two driving forces, ΔK and K_{max},

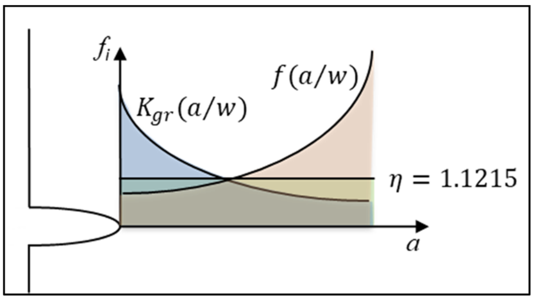

Fig. 2. Free surface η, geometry *f(a/w)*, and stress gradient $K_{gr}(a/w)$ factors.

Table 1
Main characteristics of K_I, K_t, K_f, and K_{gr}.

	Definition	Equation	Applicability
K_I	Stress Intensity Factor (Mode I)	$\sigma\sqrt{\pi a}\cdot\prod f_i$	da/dN, crack propagation
K_t	Stress Concentration Factor	σ_{max}/σ	εN, SN, crack initiation
K_f	Fatigue Notch Factor	$\frac{unnotched \quad fatigue \quad strength}{notched \quad fatigue \quad strength}$	SN, crack initiation
$K_{gr}(a/w)$	Stress Gradient Factor	$\frac{(notched) \quad K_I}{(unnotched) \quad K_{I(ref)}}$	Short crack initiation and propagation

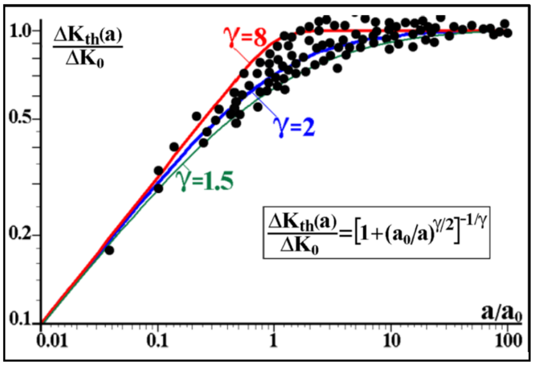

Fig. 3. Short-crack to long-crack FCG thresholds ratio as a function of a_0/a [4].

thus Eq. (5) should be generalized to include the effect of K_{max} on the behavior of short cracks, as proposed by Yu, DuQuesnay and Topper [43]. This second driving force effect can be indirectly quantified by the stress ratio R, resulting in\&&&

$$\begin{aligned} \Delta K_{th,R}(a,\, a_R) &= \Delta K_{th,R}\cdot[1+(a_R/a)^{\gamma/2}]^{-1/\gamma} \\ a_R &= \left(\frac{1}{\pi}\right)\left(\frac{\Delta K_{th,R}}{\eta\Delta S_{L,R}}\right)^2 \end{aligned} \tag{7}$$

where the free surface factor is included in the a_R equation (the characteristic short crack size at a given R) [6]. Therefore, a short crack departing from a surface notch should propagate when its (material-independent) SIF is greater than $\Delta K_{th,R}(a)$

$$\Delta K_I = \underbrace{\Delta\sigma\sqrt{\pi a}\cdot\eta}_{\Delta K_{I(ref)}}\cdot f(a/w)\cdot K_{gr}\left(\frac{a}{w}\right) > \Delta K_{th,R}(a,\ \ a_R) \tag{8}$$

For short cracks $f(a/w \to 0) = 1$, only the surface free factor remains in the reference SIF. The propagation criterion can be rewritten in terms of the stress gradient factor $K_{gr}(a/w)$ and a dimensionless function g. Considering $\Delta K_{th,R} = \eta\cdot\Delta S_{L,R}\sqrt{\pi a_R}$, then:

$$K_{gr}(a/w) \ > \ \underbrace{\frac{\Delta S_{L,R}}{\Delta\sigma}}_{K_f} \ \sqrt{\frac{a_R}{a}}\frac{1}{[1+(a_R/a)^{\gamma/2}]^{1/\gamma}} \equiv g\left(\frac{\Delta S_{L,R}}{\Delta\sigma},\ \frac{a_R}{a},\ \gamma\right) \tag{9}$$

The main idea behind Eqs. (8) and (9) was also used by Yates and Brown [44] and by Tanaka and Nakai [45]. Nonetheless, the equations presented herein are more complete, with the addition of terms such as γ. Furthermore, they allow the direct extraction of the K_f expression, whose usefulness will be later discussed in this article.

Following Castro et al. reasoning [6], a maximum crack size a_{max} limits the propagation/non-propagation condition of short fatigue cracks, satisfying Eq. (9) for any given material/stress pair. The smallest nominal stress range $\Delta\sigma_n$ that can cause crack initiation and growth without arrest is associated with the fatigue limit of the pair. Hence, the ratio $\Delta S_{L,R}/\Delta\sigma_n$ associated with a_{max} is equal to the fatigue SCF K_f. Therefore, K_f and a_{max} can be estimated from the smooth specimen fatigue limit $\Delta S_{L,R}$, the long crack FCG threshold $\Delta K_{th,R}$, and the geometry of a component, by solving the system of equations:

$$\begin{cases} \frac{K_{gr}}{g} = 1 \\ \frac{\partial}{\partial a}\left(\frac{K_{gr}}{g}\right) = 0 \end{cases} \Rightarrow \begin{cases} K_{gr}(a_{max}/w) = g(K_f,\, a_R/a_{max},\, \gamma) \\ \frac{\partial}{\partial a}[K_{gr}(a_{max}/w)] = \frac{\partial}{\partial a}[g(K_f,\, a_R/a_{max},\, \gamma)] \end{cases} \tag{10}$$

Furthermore, it is possible to obtain K_f and a_{max} by first deriving $g(K_f, a_R/a_{max}, \gamma)$

$$\frac{\partial K_{gr}(a_{max}/w)}{\partial a} = \frac{\partial g}{\partial a} = -K_f \frac{a_R}{2a_{max}^2 \eta \sqrt{a_R/a_{max}}} [1 + (a_R/a_{max})^{\gamma/2}]^{\left(-\frac{1+\gamma}{\gamma}\right)} \tag{11}$$

and then by expressing K_f in terms of the derivate $\partial K_{gr}/\partial a$ from Eq. (11):

$$K_f = -\frac{\partial K_{gr}(a_{max}/w)}{\partial a} \frac{2a_{max}^2 \eta \sqrt{a_R/a_{max}}}{a_R} [1 + (a_R/a_{max})^{\gamma/2}]^{\left(\frac{1+\gamma}{\gamma}\right)} \tag{12}$$

Substituting Eq. (12) into Eq. (10), a_{max} can be computed solving a simple non-linear equation (instead of a non-linear system of equations)

$$K_{gr}(a_{max}/w) + 2a_{max}[1 + (a_R/a_{max})^{\gamma/2}] \frac{\partial K_{gr}(a_{max}/w)}{\partial a} = 0 \tag{13}$$

After obtaining the value of a_{max}, K_f is finally computed using Eq. (9):

$$K_f = K_{gr}(a_{max}/w) \underbrace{\frac{[1 + (a_R/a_{max})^{\gamma/2}]^{1/\gamma}}{\sqrt{a_R/a_{max}}}}_{short\ crack\ factor} \tag{14}$$

It is noteworthy that the stress concentration factor under fatigue condition is a K_{gr} function obtained at a_{max} in terms of an a_R/a_{max} ratio for a given γ exponent. Fig. 4 illustrates such factor, for expected a_R/a_{max} ratios between 0.5 and 3 and γ exponents 1.5, 2, 4, 6, and 8.

3. Numerical implementation

Eqs. (13) and (14) proposed to compute K_f consider the SGF and its derivative. Although it may be possible to obtain K_f analytically or empirically, most practical calculations need to use some numerical method, so this section presents an efficient computational approach to do so. It uses the weight functions concept, calculating SIFs using the stress distribution on the crack faces. Nonetheless, SIFs may also be calculated in a simpler way by summing up all the forces applied to the crack faces, as shown in Fig. 5 [46].

In a more general way, consider a notched component submitted to an axial force F and a moment M, according to Fig. 6(a). To obtain the SIF of a crack that departs from the notch tip in this situation, the stress distribution ahead of the notch tip should be transformed into discretized forces applied to the crack face, to use the equation listed in Fig. 5 by summing the SIFs of all discretized forces. The reference geometry of Fig. 6 considers also the same axial force and moment, producing a linear stress distribution, as shown in Fig. 6(b), to compute as well the reference SIF. If the first figure gives the SIF for a notched geometry and the second gives the reference SIF, then Eq. (4) gives the SGF. In fact, to compute the SGF, it is necessary only to use the stress distributions of Fig. 6.

Discretized stresses induced by the stress concentration distribution ahead of the notch tip, see Fig. 6(a), as well as the nominal stress distribution in the un-notched strip, see Fig. 6(b), must be known. These sets of stresses and positions (σ_i, x_i) for both geometries may be obtained analytically or numerically. If the crack is considered to be parallel to the x-axis, then its length discretized segments, a_i, the mean force in a discretized face, P_i, and the mean distance between the mean force and the free surface, d_i, can be computed by:

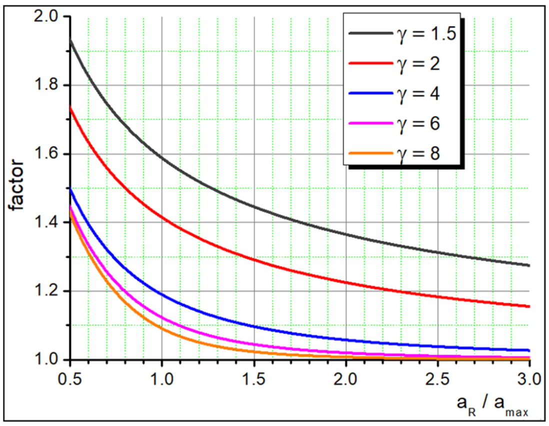

Fig. 4. Effect of the γ factor in Eq. (12) for K_f, as a function of the a_R/a_{max} ratio.

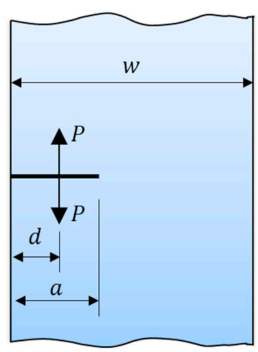

$$K_I = \frac{P}{t\sqrt{\pi a}} \frac{2\left[f_0 + f_1\left(\frac{d}{a}\right) + f_2\left(\frac{d}{a}\right)^2 + f_3\left(\frac{d}{a}\right)^3\right]}{\left(1-\frac{a}{w}\right)^{1.5}\left[1-\left(\frac{d}{a}\right)^2\right]^{1.5}}$$

$$f_0 = 0.46 + 6.06\left(\frac{a}{w}\right) + 0.84\left(1-\frac{a}{w}\right)^5 + 0.66\left(\frac{a}{w}\right)^2\left(1-\frac{a}{w}\right)^2$$

$$f_1 = -3.52\left(\frac{a}{w}\right)^2$$

$$\begin{aligned} f_2 = {} & 6.17 - 28.22\left(\frac{a}{w}\right) + 34.54\left(\frac{a}{w}\right)^2 - 14.39\left(\frac{a}{w}\right)^3 - \left(1-\frac{a}{w}\right)^{1.5} \\ & - 5.88\left(1-\frac{a}{w}\right)^5 - 2.64\left(\frac{a}{w}\right)^2\left(1-\frac{a}{w}\right)^2 \end{aligned}$$

$$\begin{aligned} f_3 = {} & -6.63 + 25.16\left(\frac{a}{w}\right) - 31.04\left(\frac{a}{w}\right)^2 + 14.41\left(\frac{a}{w}\right)^3 \\ & + 2\left(1-\frac{a}{w}\right)^{1.5} + 5.04\left(1-\frac{a}{w}\right)^5 \\ & + 1.98\left(\frac{a}{w}\right)^2\left(1-\frac{a}{w}\right)^2 \end{aligned}$$

Fig. 5. Mode I SIF for a strip with a crack loaded by concentrated forces on its face [46].

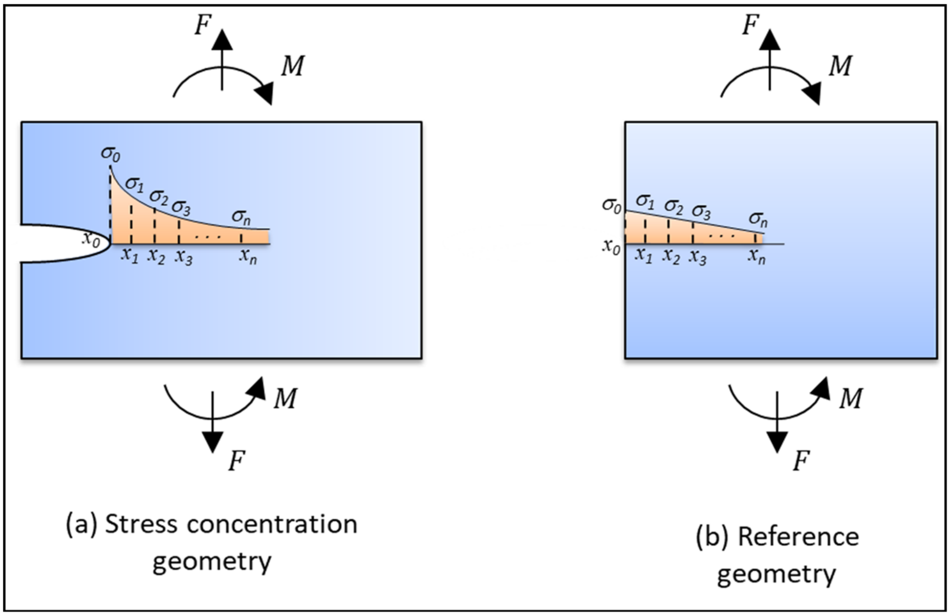

Fig. 6. Schematic stress distributions for finite strips loaded by an axial force and by a moment: (a) notched strip and (b) un-notched used as a reference geometry.

$$\begin{aligned} a_i &= x_{i+1} - x_0 \\ P_i &= \tfrac{(\sigma_{i+1}+\sigma_i)}{2}(x_{i+1} - x_i) \quad i = 0 \ldots n-1 \\ d_i &= \tfrac{(x_{i+1}+x_i)}{2} - x_0 \end{aligned} \tag{15}$$

For each crack size a_i, the SIF is computed by summing up all contributions of forces P_i applied to the face of the crack:

$$K_{I,i} = \sum_{j=0}^{j=i} K_I(P_j, t, w, d_j, a_i) \quad for \quad i = 0 \cdots n-1 \tag{16}$$

The SGF can then be obtained from the ratio of the SIFs computed for both geometries by:

$$K_{gr,i} = \frac{K_{I,i}\ (stress\ \ concentration)}{K_{I,i}(reference)} \quad for \quad i = 0 \cdots n-1 \tag{17}$$

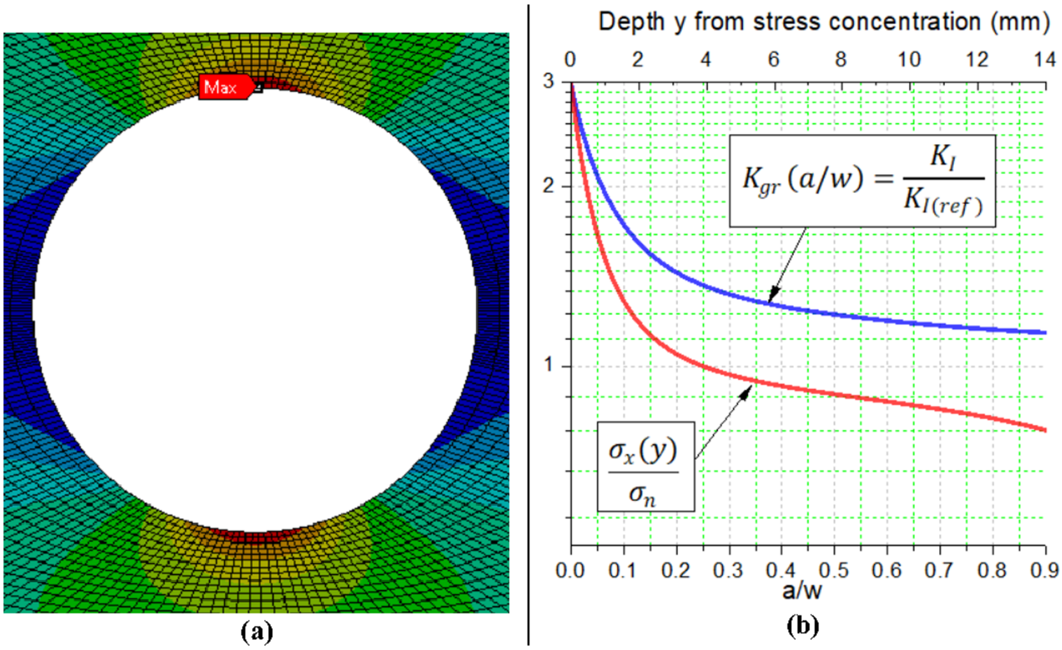

Fig. 7. (a) Example of a FE mesh and axial stress results, and (b) difference between the axial stress and stress gradient factor distributions (notice that it is not possible to assume they are equal or even similar.).

If finite differences are used to approximate $\partial K_{gr}/\partial a$, then

$$\frac{\partial K_{gr}}{\partial a} \approx \frac{K_{gr,i} - K_{gr,i-1}}{a_i - a_{i-1}} \quad for \quad i = 1 \cdots n - 1 \tag{18}$$

and Eq. (11) gives a value for each crack size expressed as

$$f_i = K_{gr,i} + 2a_i[1 + (a_R/a_i)^{\gamma/2}]\left(\frac{K_{gr,i} - K_{gr,i-1}}{a_i - a_{i-1}}\right) \quad for \quad i = 1 \cdots n - 1 \tag{19}$$

Finally, when $f_i \cdot f_{i-1} \le 0$, values of a_{max} and K_f are computed by:

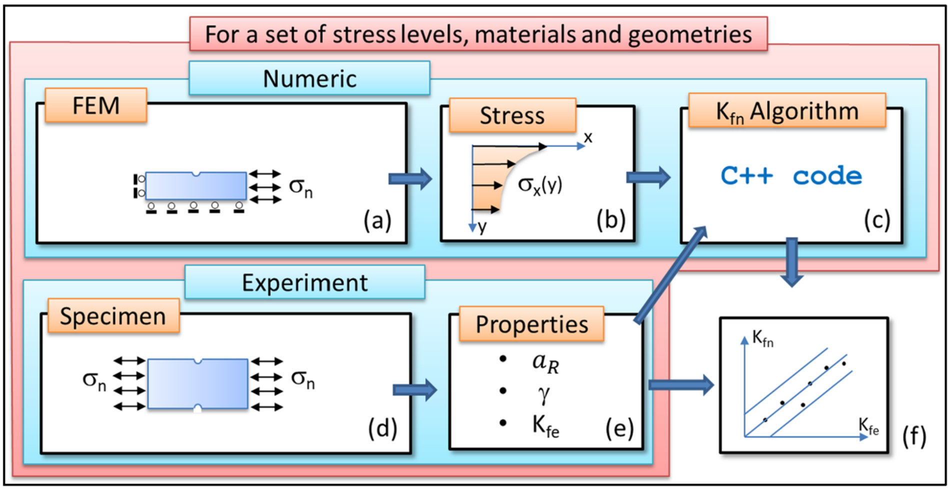

Fig. 8. Procedure to compare numerical and experimental K_f results.

$$a_{max} = a_i - f_i\left(\frac{a_i - a_{i-1}}{f_i - f_{i-1}}\right),\ K_f = K_{gr,i}\frac{[1 + (a_R/a_{max})^{\gamma/2}]^{1/\gamma}}{\sqrt{a_R/a_{max}}} \quad (20)$$

Eqs. (19) and (20) can be implemented in any computer language. Appendix A presents a simple C++ code that returns K_f values from the stress distribution, nominal stress, component geometry, and γ exponent. For example, Fig. 7(a) shows a plate with a hole submitted to a remote axial stress in the horizontal direction. Fig. 7(b) shows the horizontal axial stress in the depth (y) direction from the notch face and the SGF distribution obtained using Eq. (17).

4. Validation

Fig. 8 shows the procedure used in this study to compare numerical and experimental K_f values. It starts with the creation of numerical FE models shown in Fig. 8(a), based on the component geometries and loads shown in Fig. 8(d), to obtain the stress fields depicted in Fig. 8(b). The fatigue parameters must be obtained from experiments, as schematized in Fig. 8(e). The stress fields and the fatigue parameters are then used as inputs for the C++ code mentioned in Fig. 8(c), which computes K_f to compare it with experimental ones in Fig. 8(f). For practical applications, this procedure is repeated for each geometry, material, and load configuration.

4.1. CNBT, CNPT, and DNPT specimens

The experimental results used in this subsection were reported by Atzori et al. [47] and also used by Liu and Mahadevan [20] to validate their methodology against experimental K_f. Some of these data were also used by Sadananda et al. [48] in order to determine whether a crack propagates or not. The obtained results are contrasted with two other approaches, one reported by Liu and Mahadevan [20], and the second as the Direct Stress Gradient Method (DSGM), which is, in fact, a simplification of Eq. (14), eliminating the factor γ and assuming $a_{max} = a_R$. The specimen geometries are: circumferential V-shaped notch in a round bar under remote tension (CNBT); center-notched plate under remote tension (CNPT); and double edge notched plate under remote tension (DNPT). Fig. 9 shows the geometry and loads of these three specimens. Table 2 lists the description of materials and its fatigue properties.

Tables 3–6 show K_f's predicted by different methods for the CNPT, CNBT and DNPT specimens evaluated in this work according to their respective R load ratios. They list the difference between experimental K_f's against the Liu and Mahadevan, the SGM, and the DSGM predictions. All results are summarized in Table 7, showing the average and standard deviation of the various predictions when compared to experimentally measured K_f values. Fig. 10 plots the results for each method evaluated here. It is possible to see a very small difference between the SGM and the DSGM results.

All predictions for the CNPT specimens in Table 7 are very conservative for $R = 0$, with the SGM yielding the most conservative results. For $R = -1$, the SGM-predicted results are closer to the experimental data, but with a scatter larger than the other two

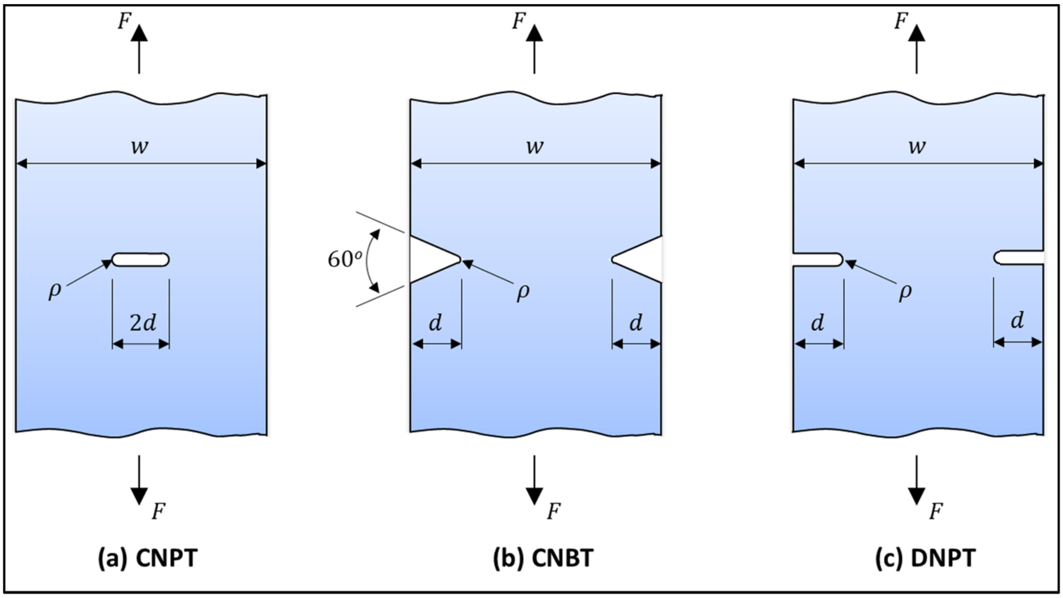

Fig. 9. The so-called CNPT, CNBT, and DNPT specimens analyzed in this work.

Table 2
Material properties of CNPT, CNBT and DNPT specimens.

Material	Yield strength (MPa)	Fatigue Limit (MPa)	Fatigue threshold SIF (MPa $\sqrt{m}$)	Stress ratio R
SAE 1045 steel	466	448	6.9	0
SAE 1045 steel	466	606	9	−1
2024- T351 Al alloy	360	172	4	0
2024- T351 Al alloy	360	248	4.4	−1
G40.11 Steel	376	540	11.5	−1
SM41B Steel	194	326	12.36	−1
SM41B Steel	194	274	8.36	0
Mild steel (0.15% C)	340	420	12.8	−1
NiCr steel	845	1000	12.8	−1
2.25 Cr-1Mo steel	380	440	12	−1
304 stainless steel	222	720	12	−1

Table 3
Comparison of results for CNPT specimens, $R = 0$.

Material	Geometry (mm)			K_f				Difference to Experiments (%)			a_{max} (mm) Eq. (13)
	d	ρ	W	Exp.	LM	SGM	DSGM	LM	SGM	DSGM	
1045 steel	0.120	0.120	44.450	1.379	1.630	1.958	1.793	18.208	42.065	30.044	0.076
1045 steel	0.250	0.250	44.450	1.455	2.022	2.361	2.162	38.989	62.315	48.670	0.071
1045 steel	0.500	0.500	44.450	1.659	2.322	2.640	2.446	39.939	59.083	47.414	0.058
1045 steel	1.500	1.500	44.450	2.113	2.637	2.739	2.630	24.763	29.598	24.448	0.039
1045 steel	2.500	2.500	44.450	2.144	2.746	2.667	2.594	28.094	24.431	21.021	0.033
2024-T351	0.120	0.120	44.450	1.000	1.196	1.804	1.653	19.610	80.402	65.295	0.109
2024-T351	0.250	0.250	44.450	1.522	1.579	2.206	2.016	3.738	44.918	32.451	0.104
2024-T351	0.500	0.500	44.450	1.608	1.960	2.537	2.330	21.935	57.828	44.962	0.076
2024-T351	1.500	1.500	44.450	2.005	2.424	2.707	2.576	20.891	35.024	28.517	0.058

Table 4
Comparison of results for CNPT specimens, $R = -1$.

Material	Geometry (mm)			K_f				Difference to Experiments (%)			a_{max} (mm) Eq. (13)
	d	ρ	W	Exp.	LM	SGM	DSGM	LM	SGM	DSGM	
1045 steel	0.120	0.120	44.450	1.698	1.670	2.000	1.832	−1.62	17.81	7.92	0.074
1045 steel	0.250	0.250	44.450	1.980	2.057	2.402	2.201	3.84	21.29	11.13	0.065
1045 steel	0.500	0.500	44.450	2.220	2.340	2.640	2.446	5.41	18.91	10.19	0.058
1045 steel	1.500	1.500	44.450	2.623	2.650	2.745	2.642	1.01	4.62	0.72	0.036
1045 steel	2.500	2.500	44.450	2.612	2.750	2.671	2.602	5.28	2.24	−0.39	0.030
2024-T351	0.120	0.120	44.450	1.560	1.472	1.561	1.431	−5.65	0.08	−8.27	0.173
2024-T351	0.250	0.250	44.450	2.016	1.878	1.894	1.740	−6.87	−6.06	−13.69	0.176
2024-T351	0.500	0.500	44.450	2.050	2.207	2.263	2.076	7.66	10.42	1.30	0.172
2024-T351	1.500	1.500	44.450	2.959	2.559	2.604	2.439	−13.54	−12.01	−17.57	0.121
G40.11 steel	0.200	0.200	70.000	1.607	1.552	0.939	0.862	−3.40	−41.57	−46.35	0.159
G40.11 steel	0.480	0.480	70.000	2.259	2.024	2.357	2.161	−10.43	4.33	−4.37	0.139
G40.11 steel	4.800	4.800	70.000	2.634	2.713	2.612	2.542	2.98	−0.84	−3.51	0.064
SM41B steel	3.000	0.160	45.000	3.421	3.615	3.033	2.890	5.67	−11.32	−15.52	0.712
SM41B steel	3.000	0.390	45.000	3.135	3.479	2.996	2.812	10.99	−4.42	−10.30	0.658
SM41B steel	3.000	0.830	45.000	3.421	3.144	2.884	2.667	−8.09	−15.71	−22.03	0.553
SM41B steel	3.000	3.000	45.000	2.547	2.320	2.384	2.216	−8.90	−6.38	−13.00	0.352
SM41B steel	3.000	0.160	45.000	4.329	4.503	3.674	3.460	4.04	−15.12	−20.07	0.379

methods. Results reported by Liu and Mahadevan [20] are slightly closer to the experimental ones as well as more conservative and less scattered. In the case of CNBT specimens, the SGM outperformed the others on average, with similar scatter in comparison to LM's and the SGF. Furthermore, all methodologies were non-conservative for such specimens. Finally, for the DNPT results, the DSGM presented the best average and the second smallest scatter. Although the SGM provided higher average (in modulus) and deviation than LM, the latter was the only non-conservative methodology for such specimens.

When the experiments are analyzed separately for each R ratio, it becomes clear from Tables 4–7 that the worst prediction scenario occurred for $R = 0$; the same is observed from the model proposed by Liu and Mahadevan [20]. For a given maximum

Table 5
Comparison of results for CNBT specimens, $R = -1$.

Material	Geometry (mm)			K_f				Difference to Experiments (%)			a_{max} (mm) Eq. (13)
	d	ρ	W	Exp.	LM	SGM	DSGM	LM	SGM	DSGM	
Mild steel (0.15% C)	5.080	0.050	43.000	6.105	5.437	6.019	5.723	−10.94	−1.41	−6.26	0.337
Mild steel	5.080	0.100	43.000	6.000	5.437	5.947	5.636	−9.39	−0.89	−6.07	0.380
Mild steel	5.080	0.130	43.000	6.204	5.436	5.969	5.653	−12.37	−3.79	−8.88	0.380
Mild steel	5.080	0.250	43.000	6.105	5.407	5.756	5.403	−11.43	−5.71	−11.50	0,380
Mild steel	5.080	0.640	43.000	6.105	5.060	5.273	4.834	−17.11	−13.62	−20.82	0.379
Mild steel	5.080	1.270	43.000	5.455	4.476	4.599	4.230	−17.93	−15.68	−22.46	0.259
Mild steel	5.080	5.080	43.000	3.471	3.041	3.129	2.991	−12.40	−9.85	−13.83	0.164
NiCr steel	0.510	0.130	22.600	4.237	3.444	3.883	3.563	−18.72	−8.37	−15.91	0.054
NiCr steel	5.080	0.050	43.000	11.287	12.435	13.372	12.546	10.17	18.47	11.16	0.074
NiCr steel	5.080	0.130	31.800	10.352	12.319	9.438	8.663	19.00	−8.83	−16.32	0.054
2.25Cr-1Mo	0.030	0.030	5.000	1.026	1.106	1.154	1.085	7.83	12.51	5.76	0.171
2.25Cr-1Mo	0.050	0.050	5.000	1.092	1.159	1.232	1.140	6.17	12.81	4.42	0.176
2.25Cr-1Mo	0.070	0.070	5.000	1.371	1.211	1.305	1.194	−11.64	−4.82	−12.93	0.177
2.25Cr-1Mo	0.200	0.200	5.000	1.857	1.526	1.630	1.495	−17.79	−12.20	−19.45	0.248
2.25Cr-1Mo	0.400	0.400	5.000	2.105	1.979	2.020	1.857	−5.99	−4.06	−11.82	0.260
2.25Cr-1Mo	0.760	0.760	5.000	2.839	2.817	2.671	2.453	−0.77	−5.92	−13.57	0.259
304 stainless	5.080	0.050	43.000	9.959	9.705	12.873	12.332	−2.55	29.27	23.83	0.126

Table 6
Comparison of results for DNPT specimens, $R = -1$.

Material	Geometry (mm)			K_f				Difference to Experiments (%)			a_{max} (mm) Eq. (13)
	d	ρ	W	Exp.	LM	SGM	DSGM	LM	SGM	DSGM	
Mild steel (0.15% C)	5.080	0.100	64.000	4.994	4.780	5.777	5.502	−4.29	15.67	10.16	0.380
Mild steel	5.080	0.250	64.000	4.621	4.750	5.623	5.299	2.80	21.69	14.68	0.379
Mild steel	5.080	0.500	64.000	4.994	4.560	5.225	4.858	−8.69	4.62	−2.73	0.375
Mild steel	5.080	1.270	64.000	4.039	3.830	4.415	4.064	−5.16	9.32	0.63	0.262
Mild steel	5.080	7.620	64.000	2.692	2.380	2.613	2.528	−11.60	−2.94	−6.11	0.146

Table 7
Comparison of K_f results for CNPT, CNBT and DNPT specimens.

Specimen	Statistical Parameter	Difference to experiments (%)		
		LM	SGM	DSGM
CNPT $R = 0$	Average	24.02	48.41	38.09
	Standard Deviation	11.03	17.96	14.37
CNPT $R = -1$	Average	−0.68	−1.98	−8.46
	Standard Deviation	7.21	15.39	14.20
CNBT $R = -1$	Average	−6.23	−1.30	−7.92
	Standard Deviation	11.21	12.35	12.46
DNPT $R = -1$	Average	−5.39	9.67	3.33
	Standard Deviation	5.43	9.55	8.78

nominal stress, $R = 0$ results in shorter fatigue lives than $R = -1$ [49]. A large part of this phenomenon can be attributed to the plasticity induced by the notch and the crack tip, which is considerably more significant for the former ratio. Furthermore, as stated by Tanaka and Nakai [45], it can be expected that notch plasticity contributes to increase the growth rate of a very short crack, especially under higher stress levels.

4.2. Non-propagating crack specimens

To validate the largest non-propagating crack size $a_{non\text{-}prop}$, which limits the propagation/non-propagation condition of short fatigue cracks that satisfies Eq. (9) for a given material/stress pair, 23 numerical models were created using Eq. (20) with $\gamma = 8$ for data found in the literature. The comparison of these results to the ones reported experimentally is displayed in Table 8.

Notice that some data seem to be inconsistent or too scattered due to the statistical nature of fatigue. The non-propagating crack size reported by Frost [50] for the mild steel ENP geometry at $\Delta\sigma = 77.8$ MPa is surprisingly larger than at $\Delta\sigma = 84.7$ MPa and much

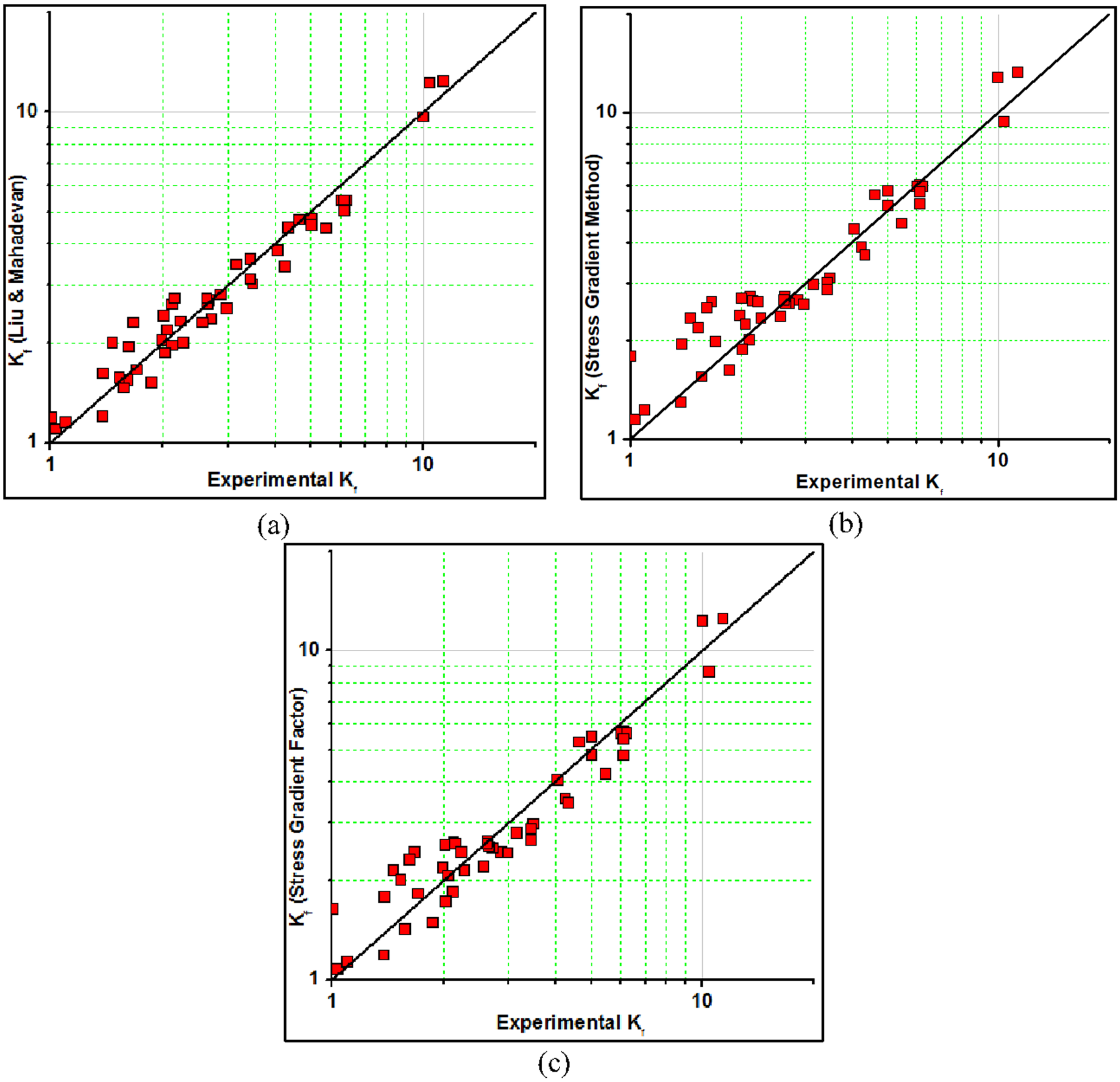

Fig. 10. Comparison between experimental K_f reported by Atzori et al. [47] and (a) Liu & Mahadevan, (b) Stress Gradient Method, and (c) Direct Stress Gradient Method predictions.

larger than at $\Delta\sigma$ = 64.9 MPa. The same inconsistency can be observed in the later reports made by Frost [51], also for mild steel ENP geometry specimens in fully reversed load, for $\Delta\sigma$ = 30.6 and $\Delta\sigma$ = 57.8 MPa. In the work of Tanaka [45], this only occurred in a single case, in which the non-propagating crack size for the CNP specimen submitted to 88.4 MPa was very different from other similar experiments.

Overall, the proposed methodology reasonably predicted non-propagating crack lengths, except when compared to the results reported by Frost [50,51]. In these cases, although some predicted values were very close to the ones observed experimentally, the proposed method was usually overconservative or predicted a too small non-propagating crack length. However, most of the failed predictions occurred for the aforementioned scattered or inconsistent data. Moreover, these studies did not include threshold stress intensity factors for the material used and they were taken as twice the maximum stress intensity factor, as assumed by Yates and Brown [44].

4.3. CT-like specimens

Additionally, CT-like specimens with an elongated notch machined from a 76.2 mm × 12.7 mm flat bar of SAE 1020 low carbon steel were tested to verify their fatigue limit predictions. The mechanical properties of this material, measured in a 100 kN Instron electromechanical testing machine at a crosshead speed of 0.9 mm/min according ASTM E8M-13a standard procedures, are: yield strength S_Y = 313 MPa, ultimate strength S_U = 490 MPa and Young Modulus E = 197 GPa. Its % chemical composition is: 0.36 Mn,

Table 8
Comparison of estimated non-propagating crack lengths to experimental data.

Material	Geometry*	R	Notch depth (mm)	Δσ (MPa)	$a_{non\text{-}p}$** (mm)	$a_{non\text{-}p\text{-}estimate}$ (mm)
Mild Steel [50]	ENP	−1	5.08	64.9	0.330	0.275
	ENP	−1	5.08	77.8	2.400	Propagates
	ENP	−1	5.08	84.7	0.500	Propagates
Mild Steel [51]	ENP	−1	20.32	27.8	0.575***	0. 220
	ENP	−1	20.32	30.6	0.350***	0.405
	ENP	−1	20.32	38.9	0.675***	Propagates
	ENP	−1	10.16	42	0.500***	0.175
	ENP	−1	10.16	57.8	0.125***	Propagates
	ENP	−1	15	30.9	0.050***	0.203
JIS SM 41B Steel [45]	CNP	−1	3	52	0.000	0.096
	CNP	−1	3	60.7	0.099	0.146
	CNP	−1	3	69.3	0.280	0.208
	CNP	−1	3	86.7	0.500	0.408
	CNP	−1	3	88.4	1.410	0.442
	CNP	0	3	42.5	0.000	0.087
	CNP	0	3	52	0.039	0.156
	CNP	0	3	60.7	0.250	0.258
	CNP	0.4	3	33.8	0.000	0.058
	CNP	0.4	3	32.3	0.029	0.133
	CNP	0.4	3	52	0.125	0.325
	CNP	0.4	3	60	0.370	Propagates
G80.11 Steel [39]	CNP	−1	0.2	241	0.066	0.102
	CNP	−1	0.2	310	0.201	Propagates

* ENP = edge notched plate, CNP = center notched plate.
** Non-propagating crack length.
*** The mean values for the four reported crack sizes were considered.

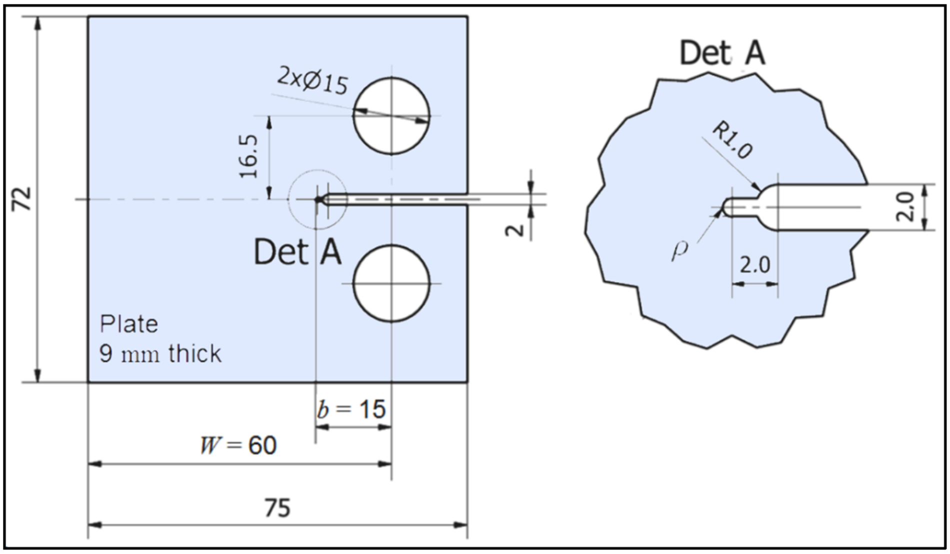

Fig. 11. Geometry and notch detail of CT specimen.

0.24 Si, 0.20 C, 0.19 Cr, 0.10 Cu, and 0.04 Ni. The grain size for this steel, determined according to ASTM-E112 standard, is G 7.0, which corresponds to an average diameter of about 32 µm.

The fatigue limit predictions were made using the characteristic crack size $a_{0.1}$, which is estimated from the smooth specimen fatigue limit, $\Delta S_{0.1}$ = 357 MPa, and the long crack propagation threshold, $\Delta K_{0.1}$ = 10 MPa√m, both of them at $R = 0.1$. The former was measured by the infrared thermography method based on the approach proposed by Risitano and Risitano [52]. Seven specimens machined according to the ASTM E606M-12 standard were tested. $\Delta K_{0.1}$ was measured according to ASTM E647 procedures by testing standard CT specimens under K-decreasing and K-increasing methods. From the measured $\Delta S_{0.1}$ and $\Delta K_{0.1}$ values, the characteristic crack size is calculated from Eq. (7) as $a_{0.1}$ = 199 µm.

The width and thickness of the C(T)-like specimens, W = 60 mm and B = 9 mm, respectively, are shown in Fig. 11. The depth

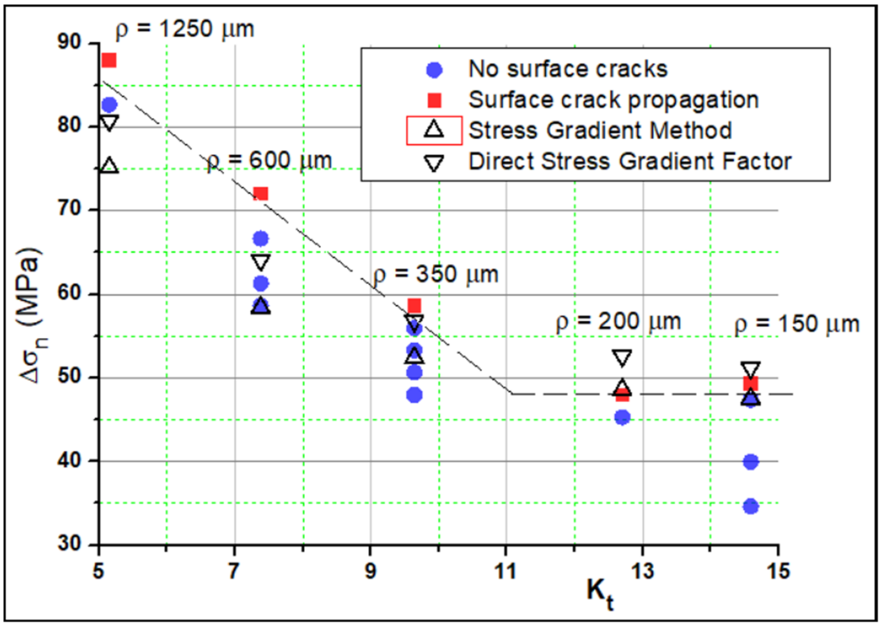

Fig. 12. Frost diagram for CT specimen tests.

Table 9
K_f measured for the CT-like notched specimens and their K_t.

Notch ratio (mm)	FEM K_t	a_{max} (mm) Eq. (13)	K_f		$\Delta S_{0.1}$	
			SGM	DSGM	SGM	DSGM
0.150	14.59	0.224	7.51	6.97	47.54	51.22
0.200	12.7	0.221	7.34	6.78	48.64	52.65
0.350	9.64	0.241	6.81	6.28	52.42	56.85
0.600	7.38	0.164	6.11	5.57	58.43	64.09
1.250	5.15	0.134	4.75	4.42	75.16	80.77

b = 15 mm was kept constant and five different tip radii were chosen for the elongated notch, ρ = {0.15; 0.20; 0.35; 0.60; 1.25} mm. Their K_t values were calculated by FE models using the Quebra2D software [53,54] considering mesh adaptability [55], namely K_t = {14.59; 12.70; 9.64; 7.38; 5.15}, respectively for each notch.

The notched CT-specimens were tested under fixed force ranges at a frequency of 40 Hz in a computer-controlled servo-hydraulic testing machine. Typical fatigue limits are specified at lives of 10^6–10^7 cycles for steels, and in this work a life of $3 \cdot 10^6$ cycles was assumed for the fatigue limit of the notched specimens. An accelerated fatigue test involving step loading was carried out following procedures proposed by Nicholas [56]. The initial load level was chosen to cause a local notch root stress slightly higher than $\Delta S_{0.1}$ and it was increased by a small step between 5% and 12%, depending on the initial stress level. After subjecting a specimen to a specific load level during a block of $3 \cdot 10^6$ cycles, the notch tip surfaces were thoroughly examined using a ZEISS Axioplan 2 microscope. If no surface cracks were detected, the load was increased by one step. When a surface crack was detected, the criterion to consider it as a propagating one is that its length should be higher than a_{max}, parameter determined by the SG model. Otherwise, it was considered as a surface non-propagating crack. From Fig. 12, it is clear that for sharper notches, i.e. ρ = 150 and 200 μm, the SGM presents results closer to the ones obtained experimentally than its direct counterpart. However, the smoother the notches are, the SGM seems to lose accuracy in relation to the DSGM. The results are summarized in Table 9.

The crack detection was carried out only in SAE 1020C(T)-like specimens with a notch root radius ρ = 0.15 mm and thickness t = 9 mm. The optical micrographs of the detected non-propagating short cracks on the face of three C(T)-like specimens are shown in Fig. 13. It can be seen that the lengths of these cracks are, on average, smaller than the predicted a_{max} and slightly higher than the grain size, so the macroscopic assumptions of the model are fulfilled. However, the length values are not constant, revealing the random nature of the fatigue short cracks especially at the initial stage of nucleation and propagation.

5. Summary and conclusions

This paper presents a general methodology to obtain fatigue stress concentration factors K_f. An alternative approach, DSGM, using an in-built, simpler concept is introduced as well. 2D numerical FE models are used to compute stress fields of uncracked notched

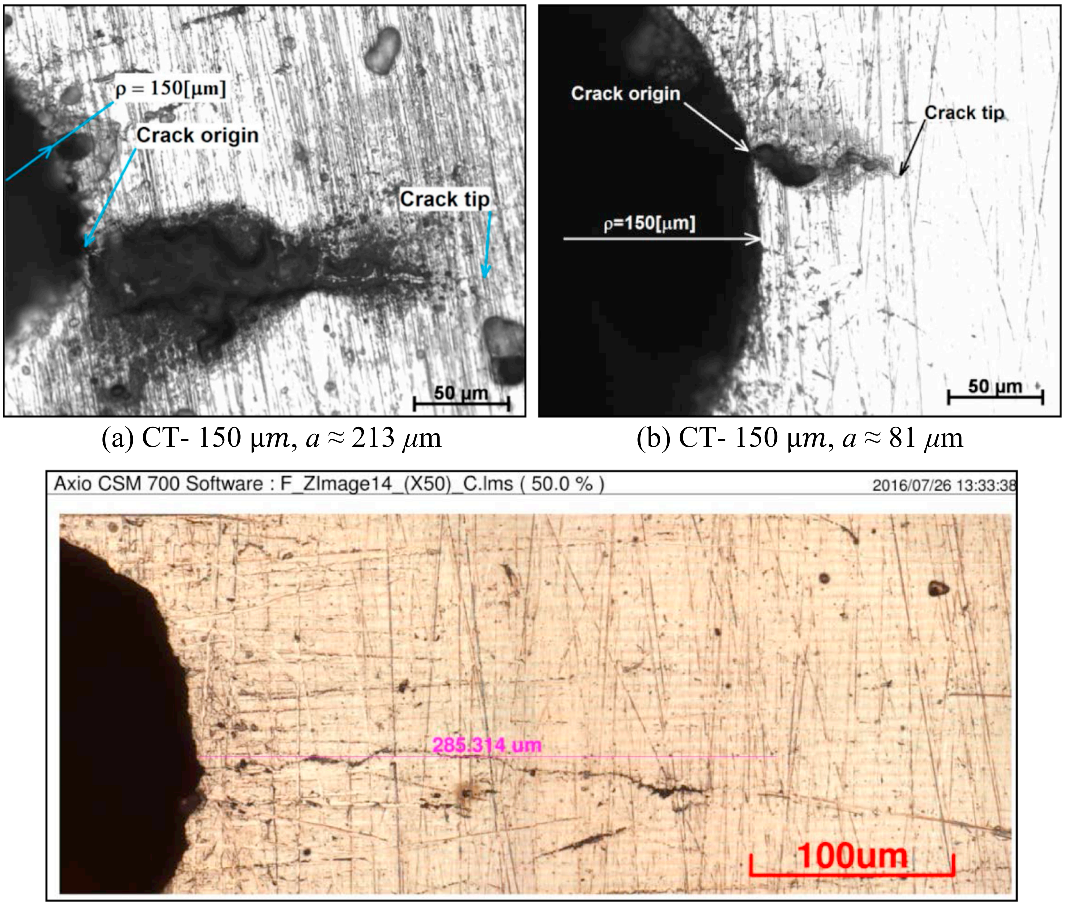

(a) CT- 150 μm, $a \approx 213$ μm (b) CT- 150 μm, $a \approx 81$ μm

(c) CT- 150 μm, $a \approx 285$ μm

Fig. 13. Optical micrographs for the three surface NPSCs detected.

pieces. To model SIFs of cracks that depart from the notch tips, weight functions are used to calculate their stress gradient factors. Such SGF are then used to compute K_f. The numerical predictions are then compared to other approaches and to experimental data. Original data is also presented and compared with the proposed methodology. A few conclusions may be drawn based on the results obtained here:

(1) There is a good agreement between the proposed methodology (and of its more direct application, the DSGM) predictions and the experimental data.
(2) The obtained predictions were, on average, closer to experimental data than the Liu & Mahadevan predictions [20], but with more scatter. However, they were more conservative than the latter approach.
(3) The presented methodology is thus a safe tool for engineers for fatigue analyses of notched components.
(4) The fatigue notch factor can be satisfactorily determined by the proposed methodology, ultimately increasing its applicability, e.g. it can be implemented in notch-analogue approaches and even incorporated into the TCD.
(5) The best predictions using the SGM occurred for sharp notches with K_f. For smoother notches or smaller K_f values, the DSGM counterpart was more accurate.

As previously stated, this study was based on 2D FE analyses using mode I SIF. Further improvements can be performed to incorporate this into 3D analyses and to consider more complex real cracks. The effects of such simplifications and how to correct them for fatigue analysis has already been reported before [31,32]. At last, the materials used in this paper are assumed elastic. Plastic effects caused by notch-induced stress gradients can be considered using, for instance, strain-based fracture mechanics concepts [30,33,37].

Appendix A. C++ code to compute K_f

```
double getKt_gradient( stressDist &data, double w, double gamma, double a0,
              double (*nominalStress) (double) )
{
  vector<double> x_pos, sigma, delta; // compute x_pos, stress, and delta
  for (size_t j = 0; j < data.len.size()-1; ++j)
  {
    x_pos.push_back((data.len[j] + data.len[j+1]) * 0.5);
    delta.push_back(data.len[j+1] - data.len[j]);
    sigma.push_back((data.stress[j] + data.stress[j+1]) * 0.5);
  }

  double k_ref, k_cur, sigma_n; // auxiliary variables
  // current and previous Kgr
  double Kgr_i = -1.0, Kgr_i_1 = -1.0; // initialize with -1
  double f_i = -1.0, f_i_1 = -1.0;     // initialize with -1
  bool comp_fi_i = false;

  // for each crack size
  for (size_t i = 1; i < data.len.size(); ++i)
  {
    double a_i = data.len[i];     // current crack length
    double a_i_1 = data.len[i-1]; // previous crack length
    double K_ref = 0, K_cur = 0;  // reference and current SIF for a crack size

    if (a_i <= 0.005) continue; // avoid very small crack

    for (size_t k = 0; k < i; ++k)
    {
      sigma_n = nominalStress(x_pos[k]); // obtain nominal stress
      // contributions of reference and current SIF
      k_cur = computeSIF (w, a_i, sigma[k]*delta[k], x_pos[k]);
      k_ref = computeSIF (w, a_i, sigma_n*delta[k],  x_pos[k]);

      K_cur += k_cur; // add SIF contribution for current crack size
      K_ref += k_ref; // add reference SIF contribution for current crack size
    }

    Kgr_i = K_cur/K_ref; // compute current Kgr
    if (Kgr_i_1 != -1.0) // check if has previous Kgr
    {
      double derive = (Kgr_i - Kgr_i_1) / (a_i - a_i_1);
      if (derive == 0)
        continue;

      double tmp = (1 + pow(a0/a_i, gamma/2));
      f_i = Kgr_i + 2 * a_i * tmp * derive;  // current value of fi

      if (f_i * f_i_1 <= 0 && f_i_1 != -1) // check if its possible to compute Kf
      {
        double a_max = a_i - f_i * (a_i - a_i_1) / (f_i - f_i_1);
        double Kf = Kgr_i * pow (tmp, 1/gamma) / sqrt(a0/a_max);
        return Kf;  // return Kf value
      }
    }
    // update previous values
    Kgr_i_1 = Kgr_i;
    f_i_1 = f_i;
  }

  return 0.0; // fail
}
```

References

[1] Taylor D. Geometrical effects in fatigue: a unifying theoretical model. Int J Fatigue 2000;21:413–20.
[2] Tovo R, Livieri P. An implicit gradient application to fatigue of complex structures. Eng Fract Mech 2008;75:1804–14.
[3] Fleck NA, Olurin OB, Chen C, Ashby MF. The effect of hole size upon the strength of metallic and polymeric foams. J Mech Phys Solids 2001;49:2015–30.
[4] Meggiolaro MA, Miranda ACO, Castro JTP. Short crack threshold estimates to predict notch sensitivity factors in fatigue. Int J Fatigue 2007;29:2022–31.
[5] Wu H, Imad A, Nouredine B, Castro JTP, Meggiolaro MA. On the prediction of the residual fatigue life of cracked structures repaired by the stop-hole method. Int J Fatigue 2010;32:670–7.
[6] Castro JTP, Meggiolaro MA, Miranda ACO, Wu H, Imad A, Nouredine B. Prediction of fatigue crack initiation lives at elongated notch roots using short crack concepts. Int J Fatigue 2012;42:172–82.
[7] Castro JTP, Meggiolaro MA. Is notch sensitivity a stress analysis problem? Fratt Integrità Strutt 2013;25:79–86.
[8] Castro JTP, Landim RV, Leite JCC, Meggiolaro MA. Prediction of notch sensitivity effects in fatigue and EAC. Fatigue Fract Eng Mater Struct 2015;38:161–79.
[9] Castro JTP, Landim RV, Meggiolaro MA. Defect tolerance under environmentally-assisted cracking conditions. Corros Rev 2015;33:417–32.
[10] Ciavarella M, Meneghetti G. On fatigue limit in the presence of notches: classical vs. recent unified formulations. Int J Fatigue 2004;26:289–98.
[11] Neuber H. Kerbspannungslehre. Springer; 1937.
[12] Peterson RE. Stress concentration factors. 2nd ed. Wiley; 1997.
[13] Heywood R. Designing against fatigue. Chapman and Hall; 1962.
[14] Juvinall RC. Stress, strain and strength. McGraw-Hill; 1967.
[15] Rice RC, editor. Fatigue design handbook. SAE; 1988.
[16] Dowling NE. Mechanical behavior of materials. 3rd ed. Prentice Hall; 2007.
[17] Castro JTP, Meggiolaro MA. Fatigue Design Techniques (3 volumes). CreateSpace 2016.
[18] Kuhn P, Hardrath HF. An engineering method for estimating notch-size effect in fatigue tests on steel. NASA Tech Note 2805; 1952.
[19] Yao W, Xia K, Gu Y. On the fatigue notch factor, K_f. Int J Fatigue 1995;17:245–51.
[20] Liu Y, Mahadevan S. Fatigue limit prediction of notched components using short crack growth theory and an asymptotic interpolation method. Eng Fract Mech 2009;76:2317–31.
[21] Navarro C, Vázquez J, Domínguez J. A general model to estimate life in notches and fretting fatigue. Eng Fract Mech 2011;78:1590–601.
[22] Zhuang W, Molent L. Analytical study of fatigue crack growth in AA7050 notched specimens under spectrum loading. Eng Fract Mech 2010;77:1884–95.
[23] Götz S, Eulitz KG. Concepts to estimate the endurance limit of notched parts-a statistical evaluation using a broad database for P/M steels. Int J Fatigue 2013;52:1–10.
[24] Lukáš P, Kunz L, Weiss B, Stickler R. Non-damaging notches in fatigue. Fatigue Fract Eng Mater Struct 1986;9:195–204.
[25] Götz S, Ellmer F, Eulitz KG. A fracture mechanics-based approach to estimating the endurance limit of notched components. Eng Fract Mech 2016;151:37–50.
[26] Yang Y, Vormwald M. Fatigue crack growth simulation under cyclic non-proportional mixed mode loading. Int J Fatigue 2017;102:37–47.
[27] Musraty W, et al. Ductile fracture of pipe-ring notched bend specimens – micromechanical analysis. Eng Fract Mech 2017;175:247–61.
[28] Zhang ZL, Thaulow C. A complete Gurson model approach for ductile fracture. Eng Fract Mech 2000;67(2):55–168.
[29] Dong Y, Garbatov Y, Guedes Soares C. A two-phase approach to estimate fatigue crack initiation and propagation lives of notched structural components. Int J Fatigue 2018;116:523–34.
[30] Ghahremani K, Walbridge S, Topper TH. A methodology for variable amplitude fatigue analysis of HFMI treated welds based on fracture mechanics and small-scale experiments. Eng Fract Mech 2016;163:348–65.
[31] Antunes MA, Silva CRM, Rêgo EMF, Miranda ACO. Stress intensity factor solutions for fretting fatigue using stress gradient factors. Eng Fract Mech 2017;186:331–46.
[32] Rêgo EMF, Antunes MA, Miranda ACO. A methodology for fretting fatigue life estimation using strain-based fracture mechanics. Eng Fract Mech 2018;194:24–41.
[33] El Haddad M, Topper TH. Fatigue life predictions of smooth and notched specimens. ASME J Eng Mater Technol 1981;103:91–6.
[34] Dabayeh AA, Xu RX, Du BP, Topper TH. Fatigue of cast aluminium alloys under constant and variable-amplitude loading. Int J Fatigue 1996;18:95–104.
[35] Dabayeh AA, Berube AJ, Topper TH. An experimental study of the effect of a flaw at a notch root on the fatigue life of cast Al 319. Int J Fatigue 1998;20:517–30.
[36] El Haddad M, Smith KN, Topper TH. A strain based intensity factor solution for short fatigue cracks initiating from notches. Fract. Mech 1979;ASTM STP 677:274–89.
[37] Meggiolaro MA, Miranda ACO, Castro JTP, Martha LF. Crack retardation equations for the propagation of branched fatigue cracks. Int J Fatigue 2005;27:1398–407.
[38] Meggiolaro MA, Miranda ACO, Castro JTP, Martha LF. Stress intensity factor equations for branched crack growth. Eng Fract Mech 2005;72:2647–71.
[39] El Haddad M, Topper TH, Smith KN. Prediction of non-propagating cracks. Eng Fract Mech 1979;11:573–84.
[40] El Haddad M, Smith KN, Topper TH. Fatigue crack propagation of short cracks. J Eng Mater Technol 1979;101:42–6.
[41] Kitagawa S, Takahashi H. Applicability of fracture mechanics to very small crack or cracks in the early stage. Int Conf Mech Behavior Mater 1976:627–31.
[42] Bažant ZP. Scaling of quasibrittle fracture: asymptotic analysis. Int J Fract 1997;83:19–40.
[43] Yu MT, DuQuesnay DL, Topper TH. Notch fatigue behaviour of SAE1045 steel. Int J Fatigue 1988;10:109–16.
[44] Yates JR, Brown MW. Non-propagating fatigue cracks. Fatigue Fract Eng Mater Struct 1987;10:187–201.
[45] Tanaka K, Nakai Y. Propagation and non-propagation of short fatigue cracks at a sharp notch. Fatigue Fract Eng Mater Struct 1983;6(4):315–27.
[46] Tada H, Paris PC, Irwin GR. The stresses analysis of cracks handbook. 3rd ed. ASME Press; 2000.
[47] Atzori B, Lazzarin P, Meneghetti G. Fracture mechanics and notch sensitivity. Fatigue Fract Eng Mater Struct 2003;26:257–67.
[48] Sadananda K, Arcari A, Vasudevan AK. Does a nucleated crack propagate? Eng Fract Mech 2017;176:144–60.
[49] Marissen ZSR, Schulte K, Trautmann KK, Nowack H, Schijve J. Crack propagation studies on basis of constant amplitude and selective variable amplitude loading histories. Fatigue Fract Eng Mater Struct 1987;10:315–32.
[50] Frost NE, Dugdale DS. Fatigue tests on notched mild steel plates with measurements of fatigue cracks. J Mech Phys Solids 1957;5:182–92.
[51] Frost NE, Eng BS, Member A. A relation between the critical alternating propagation stress and crack length for mild steel. Proc Inst Mech Eng 1959;173.
[52] Risitano A, Risitano G. L'importanza del 'parametro energetico' temperatura per la caratterizzazione dinamica dei materiali. Fratt Integrità Strutt 2009;3:113–24.
[53] Miranda ACO, Meggiolaro MA, Castro JTP, Martha LF, Bittencourt TN. Fatigue life and crack path predictions in generic 2D structural components. Eng Fract Mech 2003;70:1259–79.
[54] Miranda ACO, Meggiolaro MA, Martha LF, Castro JTP. Stress intensity factor predictions: comparison and round-off error. Comput Mater Sci 2012;53:354–8.
[55] Miranda ACO, Lira WWM, Cavalcante-Neto JB, Sousa RA, Martha LF. A three-dimensional adaptive mesh generation approach using geometric modeling with multi-regions and parametric surfaces. J Comput Inf Sci Eng 2013;13:021002.
[56] Nicholas T. High cycle fatigue: a mechanics of material perspective. Elsevier; 2006.